

# A Nonlinear Dimensionality Reduction Framework Using Smooth Geodesics

Kelum Gajamannage, Randy Paffenroth, and Erik M. Bollt

**Abstract**—Existing dimensionality reduction methods are adept at revealing hidden underlying manifolds arising from high-dimensional data and thereby producing a low-dimensional representation. However, the smoothness of the manifolds produced by classic techniques in the presence of noise is not guaranteed. In fact, the embedding generated using such non-smooth, noisy measurements may distort the geometry of the manifold and thereby produce an unfaithful embedding. Herein, we propose a framework for nonlinear dimensionality reduction that generates a manifold in terms of smooth geodesics that is designed to treat problems in which manifold measurements have been corrupted by noise. Our method generates a network structure for given high-dimensional data using a neighborhood search and then produces piecewise linear shortest paths that are defined as geodesics. Then, we fit points in each geodesic by a smoothing spline to emphasize the smoothness. The robustness of this approach for noisy and sparse datasets is demonstrated by the implementation of the method on synthetic and real-world datasets.

**Index Terms**—Manifold, nonlinear dimensionality reduction, smoothing spline, geodesics, noisy measurements.



## 1 INTRODUCTION

ADVANCED data collection techniques in today's world require researchers to work with large volumes of nonlinear data, such as global climate patterns [1], [2], satellite signals [3], [4], social and mobile networks [5], [6], the human genome [7], [8], and patterns in collective motion [9], [10]. Studying, analyzing, and predicting such large datasets is challenging, and many such tasks might be implausible without the presence of Nonlinear Dimensionality Reduction (NDR) techniques. NDR interprets high-dimensional data using a reduced dimensional representation that corresponds to the intrinsic nonlinear dimensionality of the data [11]. Manifolds are often thought of as being smooth, however many existing NDR methods do not directly leverage this important feature. Sometimes, ignoring the underlying smoothness of the manifold can lead to inaccurate embeddings, especially when the data has been contaminated by noise.

Many NDR methods have been developed over the last two decades due to the lack of accuracy and applicability of classic Linear Dimensionality Reduction (LDR) methods such as Principal Component Analysis (PCA) [12], which finds directions of maximum variance, or Multi-Dimensional Scaling (MDS) [13], which attempts to preserve the squared Euclidean distance between pairs of points. As the Euclidean distance used in MDS quantifies the distance between points in the high-dimensional space, rather the

actual distance along the manifold, it can have difficulty inferring a faithful low-dimensional embedding. On the other hand, Isometric Mapping (Isomap) represents the pairwise distance between points using *geodesic distances* and is an NDR method that successfully resolves the aforesaid problem in MDS [14]. Although Isomap has been successfully used to analyze low-dimensional embedding of data from several domains, such as collective motion [15], face recognition [16], and hand-writing digit classification [17], this method can suffer from short-circuiting [18], low-density of the data [19], and non-convexity [20], all of which can be magnified in the presence of noisy measurements. It is therefore our goal here to propose a new method which ameliorates some of these issues as compared to Isomap.

Generally speaking, NDR approaches reveal a smooth low-dimensional, nonlinear manifold representation of high-dimensional data. While there are many unique capabilities provided by current NDR methods, most of them encounter poor performance in specific instances. In particular, many current NDR methods are not adept at preserving the smoothness of the embedded manifold in the presence of noise. Specifically, Isomap closely mimics the underlying manifold's geometry using a graph structure that it makes using a neighborhood search [21], [22], over the high-dimensional data. Geodesics are generally *piecewise linear*, thus, the manifold constructed using geodesics in this method is not actually smooth at each node, as demonstrated in Fig. 1(a). Moreover, the length of such a geodesic between two points is not necessarily the manifold distance. In fact, given a sufficiently smooth manifold, the Isomap generated geodesic distance will generally be an *over-estimate* of the true manifold distance, again as demonstrated in Fig. 1(b). Of course, such issues are intensive in the presence of noisy measurements. Accordingly, herein we propose to *replace the segments of the piecewise linear Isomap geodesic by a smoothing spline* as shown by the black curve in Fig. 1(b) and *consider the length of the spline as the estimation*

- K. Gajamannage is with the Department of Mathematical Sciences, Worcester Polytechnic Institute, Worcester, MA, 01609.  
E-mail: kdgajamannage@wpi.edu
- R. Paffenroth is with the Department of Mathematical Sciences, Department of Computer Science, and Data Science Program, Worcester Polytechnic Institute, Worcester, MA, 01609.  
E-mail: rcpaffenroth@wpi.edu
- E. M. Bollt is with the Clarkson Center for Complex Systems Science, Clarkson University, Potsdam, NY, 13676.  
E-mail: ebollt@clarkson.edu

Manuscript received MONTH DATE, YEAR; revised August MONTH DATE, YEAR.

of the manifold distance between points.

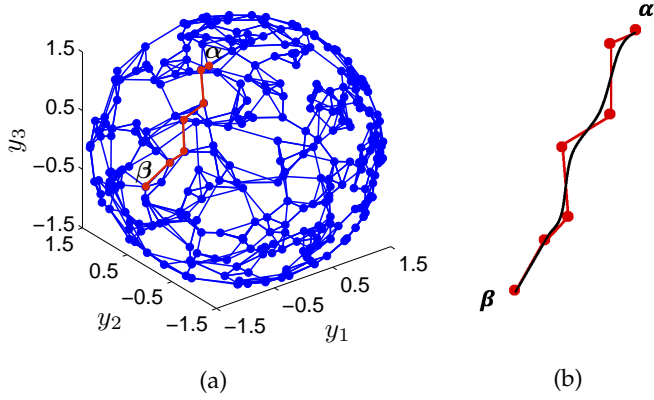


Fig. 1: This figure demonstrates the lack of smoothness of the geodesics generated by Isomap. (a) Three nearest neighbors for each point (blue dots) of a spherical dataset of 300 points are found and joined by line segments (shown in blue) to create a graph structure. The Isomap manifold distance between two arbitrary points  $\alpha$  and  $\beta$  is estimated as the length of the geodesic (red path), that is defined as the shortest path between two points, computed by using, for example, Floyd’s algorithm [23]. (b) However, our approach creates a *smoothing spline*, shown by the black curve, that is fitted through the points in the geodesic as a better approximation of the distances on the smooth manifold than the geodesic distance.

There are few NDR methods found in the literature that utilize smoothing splines for embedding like our approach. For example, Local Spline Embedding (LSE) also uses a smoothing spline to perform the embedding [24]. However, this method minimizes the reconstruction error of the objective function and embeds the data using smoothing splines that map local coordinates of the underlying manifold to global coordinates. Specifically, LSE assumes the existence of a smooth low-dimensional underlying manifold and the embedding is based on an eigenvalue decomposition that is used to project the data onto a tangent plane. However, differing from our approach, LSE assumes that the data is noise free and unaffected by anomalies. The Principal Manifold Finding Algorithm (PMFA) is another NDR method that also uses cubic smoothing splines to represent the manifold and then quantifies the intrinsic distances of the points on the manifold as lengths of the splines [25]. However, this approach embeds high-dimensional data by reducing the reconstruction error over a two-dimensional space. As this method only performs two-dimensional embeddings, its applicability is limited for problems with larger intrinsic dimensionality. As we will demonstrate in the sequel, our proposed methods overcome the limitations of these methods.

This paper is structured as follows. In Section 2, we will detail the MDS and Isomap algorithms and describe the evolution of our NDR method from these methods. Section 3 presents our NDR method, Smooth Geodesic Embedding (SGE), that fits geodesics, as in Isomap, by smoothing splines. We analyze the performance of the SGE method in Section 4 using three representative examples:

a semi-spherical dataset; images of faces; and images of hand written digits. Finally, we provide discussion and conclusions in Section 5.

## 2 MULTIDIMENSIONAL SCALING AND ISOMAP

We begin our analysis by deriving the mathematical details of the LDR method MDS. Then, we proceed to discuss Isomap which replaces the Euclidean distance in MDS by a geodesic distance. Next, we derive our method, SGE, as an extension of Isomap that fits geodesics by smoothing splines.

### 2.1 Multidimensional scaling

Multidimensional scaling is a classic LDR algorithm that leverages the squared Euclidean distance matrix  $\mathbf{D} = [d_{ij}^2]_{n \times n}$  where  $d_{ij} = \|\mathbf{y}_i - \mathbf{y}_j\|_2$  and  $n$  is the order of the high-dimensional space. Here,  $\mathbf{y}_i, \mathbf{y}_j \in \mathbb{R}^{n \times 1}$ , are two points on the high-dimensional dataset  $\mathbf{Y} = [\mathbf{y}_1; \dots; \mathbf{y}_i; \dots; \mathbf{y}_j; \dots; \mathbf{y}_n]$ . This method first transforms the distance matrix  $\mathbf{D}$  into a Gram matrix  $\mathbf{S} = [s_{ij}]_{n \times n}$ , which is derived by *double-centering* [26] the data using

$$s_{ij} = -\frac{1}{2} [d_{ij}^2 - \mu_i(d_{ij}^2) - \mu_j(d_{ij}^2) + \mu_{ij}(d_{ij}^2)]. \quad (1)$$

Here,  $\mu_i(d_{ij}^2)$  and  $\mu_j(d_{ij}^2)$  are the means of the  $i$ -th row and  $j$ -th column, respectively, of the squared distance matrix, and  $\mu_{ij}(d_{ij}^2)$  is the mean of the entire matrix  $\mathbf{D}$ . MDS then computes the Eigenvalue Decomposition (EVD) of  $\mathbf{S}$  as

$$\mathbf{S} = \mathbf{U} \mathbf{\Sigma} \mathbf{U}^T, \quad (2)$$

where  $\mathbf{U}$  is a unitary matrix ( $\mathbf{U}^T \mathbf{U} = \mathbf{I}$ ) providing the singular vectors and  $\mathbf{\Sigma}$  is a diagonal matrix of singular-values. The Gram matrix  $\mathbf{S}$ , that is made from the Euclidean distance matrix  $\mathbf{D}$ , is symmetric and positive semidefinite<sup>1</sup>. Thus, all the eigenvalues of  $\mathbf{S}$  are non-negative, and both the Singular-Value Decomposition (SVD) and the EVD of  $\mathbf{S}$  are the same [26].  $\mathbf{\Sigma}$  and  $\mathbf{U}$  are arranged such that the diagonal of  $\mathbf{\Sigma}$  contains the eigenvalues of  $\mathbf{S}$  in descending order, and the columns of  $\mathbf{U}$  represent the corresponding eigenvectors in the same order. We estimate  $p$ -dimensional latent variables of the high-dimensional dataset by

$$\hat{\mathbf{X}} = \mathbf{I}_{p \times n} \mathbf{\Sigma}^{1/2} \mathbf{U}^T. \quad (3)$$

Here,  $\hat{\mathbf{X}}$  is the  $d$ -dimensional embedding of the input data  $\mathbf{Y}$ . Note, in the case of a matrix  $\mathbf{S}$  which is not symmetric positive semidefinite, the EVD has negative eigenvalues which then violate Eqn. (3) [26]. Accordingly, as we discuss in Section 2.2, we replace the EVD computation on  $\mathbf{S}$  by SVD.

Multidimensional scaling has limited applicability as it is inherently a linear method (when  $\mathbf{D}$  is a squared Euclidean distance matrix). However, the NDR scheme Isomap overcomes this problem by employing geodesic distances instead of Euclidean distances.

1. A symmetric  $n \times n$  matrix  $\mathbf{M}$  is said to be positive semidefinite, if  $\mathbf{z}^T \mathbf{M} \mathbf{z} \geq 0$  for all non-zero  $\mathbf{z} \in \mathbb{R}^{n \times 1}$ .

## 2.2 Isomap

Isomap works by creating a graph structure, based upon high-dimensional data, that estimates the intrinsic geometry of the manifold. The graph structure used by Isomap can be parameterized in multiple ways, but herein we focus on the parameter  $\delta$  which measures the number of *nearest neighbors* to a given point [22]. The nearest neighbor collection for each point is transformed into a graph structure by treating points as graph nodes and connecting each pair of nearest neighbors by an edge having the weight equal to the Euclidean distance between the two points. Given such a graph, the distance between any two points is measured as the *shortest path distance in the graph*, which is commonly called the *geodesic distance*.

The geodesic distance between any two points in the data can be computed in many ways, including Dijkstra's algorithm [27]. We employ Floyd's algorithm [23] for this task as it computes the shortest paths between all pairs of nodes in one batch, and is more efficient than Dijkstra's algorithm in this case.

As in MDS, we first formulate the doubly centered matrix  $S$  from the squared geodesic distance matrix using Eqn. (1). Here, the doubly centered matrix is not necessarily positive semidefinite as we *approximate* the true geodesic distance matrix by the shortest graph distance [26]. Thus, the eigenvalue decomposition of the  $S$  matrix might produce negative eigenvalues and Eqn. (3) does not hold in this case. To overcome this problem, it is standard to perform the SVD over the Gram matrix  $S$  as

$$S = V\Sigma U^T, \quad (4)$$

where  $\Sigma$  is a diagonal matrix of singular values (non negative), and  $U$  and  $V$  are unitary matrices. The latent variables of the higher dimensional input data are revealed by Eqn. (3) with  $\Sigma$  and  $U^T$  obtained from Eqn. (4).

Isomap emphasizes nonlinear features of the manifold, however the lengths measured using geodesics might not faithfully reflect the correct manifold distance, as we demonstrate in Fig. 1. Accordingly, we propose to overcome this drawback in Isomap by utilizing a smoothing approach for geodesics.

## 3 SMOOTHING GEODESICS EMBEDDING

Our goal is to fit the geodesics computed in Isomap with smoothing splines to more closely mimic the manifold and preserve the geometry of the embedding. Classic smoothing spline constructions [28] require one input parameter, denoted by  $s$ , that controls the smoothness of the spline fitted through the points in a geodesic. Our proposed method, SGE, has five parameters:

- $\delta$  (inherent from Isomap) for the number of nearest neighbors,
- $\mu_s$  controls the smoothness of the splines,
- $\nu$  controls the threshold of the length of splines before reducing the order of the spline to the next level,
- $h$  controls the number of discretizations that the method uses to evaluate the length of a spline, and

- finally,  $p$  prescribes the number of embedding dimensions.

Here, we demonstrate our approach by constructing a spline on an arbitrary geodesic  $\mathcal{G}$ , having  $m \geq 2$  points, in the graph created by a neighborhood search algorithm. For an index  $k$  we have that  $d$ -dimensional points in  $\mathcal{G}$  are given by

$$\{\mathbf{y}_k = [y_{1k}, \dots, y_{dk}]^T | k = 1 \dots, m\}. \quad (5)$$

For each dimension  $l \in \{1, \dots, d\}$ , we fit  $\{y_{lk} | k = 1 \dots, m\}$  using one dimensional smoothing splines  $\hat{f}_l(z)$  of order  $\theta+1$  that are parameterized in  $z \in [0, 1]$  by minimizing

$$\sum_{k=1}^m [y_{lk} - \hat{f}_l(z_k)] + s \int_0^1 [\hat{f}_l^{(\theta)}(z)]^2 dz \quad (6)$$

as in [28]. Here,  $(\theta)$  represents the order of the derivative of  $\hat{f}_l$ , and  $z_k$  is a discretization of the interval  $[0, 1]$  such that  $z_1 = 0$ ,  $z_k = (k-1)/(m-1)$ , and  $z_m = 1$ . Minimizing of Eqn. (6) yields  $d$  one-dimensional smoothing splines  $\{\hat{f}_l(z) | l = 1, \dots, d\}$ . We combine these one dimensional splines and obtain a  $d$ -dimensional smoothing spline of the points  $\{\mathbf{y}_k | k = 1 \dots, m\}$  in  $\mathcal{G}$ ,

$$\hat{\mathbf{f}}(z) = [\hat{f}_1(z), \dots, \hat{f}_d(z)]^T, \quad (7)$$

that estimates the *smooth geodesic*. In numerical implementations, the order  $\theta+1$  of the spline  $\hat{f}$  should be less than number of points  $m$  in the geodesic [28].

Choosing the order of the spline is challenging, since while a spline with some specified order might perfectly fit the data (and thereby over-fit the noise in the data), another spline with a different order might only fit the data weakly. The length of the fitted spline between two points is defined as the manifold distance between those two points, thus either an over-fitted or under-fitted spline might provide an incorrect manifold distance. To overcome this problem, we introduce the spline threshold (in percentage) which allows the maximum length of a spline that can yield beyond the length of the geodesic. We treat the geodesic distance as the default manifold distance between two points. If the length of a spline with a specific order exceeds this limit, SGE reduces the order of the spline to the next level until the length of the spline satisfies the threshold or reaches the default length of the geodesic distance. It is worthwhile to try a spline fit with a lower order when a higher order spline fails numerically.

We present below our procedure of choosing the order of a given spline under three main cases (1, 2, and 3) and sub-cases (a, b, ...):

- **Case-1** If  $m \geq 4$ :
  - **Case-a**: we first fit the points in the geodesic with a cubic smoothing spline  $\hat{\mathbf{f}}(z)$  where  $z \in [0, 1]$  according to Eqn. (6) and Eqn. (7). Note that, a cubic smoothing spline is represented by  $\theta = 2$  in Eqn. (6). We discretize this spline into  $h$  segments  $z_{k_1} = (k_1 - 1)/(h - 1)$ ;  $k_1 = 1, \dots, h$  and compute the length,

$$d_{\hat{\mathbf{f}}} = \sum_{k_1=1}^{h-1} \|\hat{\mathbf{f}}(z_{k_1+1}) - \hat{\mathbf{f}}(z_{k_1})\|. \quad (8)$$

Then, the length  $d_{\hat{f}}$  is compared with the corresponding geodesic distance

$$d_G = \sum_{k=1}^{m-1} \|\mathbf{y}_{k+1} - \mathbf{y}_k\|. \quad (9)$$

If  $d_{\hat{f}} < d_G(100 + \nu)/100$  (so that  $\nu$  is thought of as a percentage), then we accept  $d_{\hat{f}}$  as the length of the smooth geodesic, otherwise we proceed to Case-b. The parameter  $\nu$  (in percentage) defines the threshold (the upper bound) of the length of the spline  $\hat{f}$  that is allowed to exceed from the length of the corresponding geodesic.

- **Case-b:** we fit the data with a quadratic (i.e.,  $\theta = 1$ ) spline  $\hat{f}$  according to Eqn. (6) and Eqn. (7) and compute the length of the quadratic spline using Eqn. (8). If  $d_{\hat{f}} < d_G(100 + \nu)/100$ , then we accept  $d_{\hat{f}}$  as the length of the smooth geodesic, otherwise move to the next case.
- **Case-c:** we make a linear (i.e.,  $\theta = 0$ ) fit  $\hat{f}$  according to Eqn. (6) and Eqn. (7), and measure the length using Eqn. (8). If  $d_{\hat{f}} < d_G(100 + \nu)/100$  in the linear fit, then we accept  $d_{\hat{f}}$ , otherwise we move to Case-d.
- **Case-d:** instead of fitting a spline, we consider the original geodesic itself as the fit and treat  $d_G$  as the length of the smooth geodesic.
- **Case-2** If  $m = 3$ :  
The spline fitting process here is started from fitting a quadratic spline as only three points are in the geodesic. Thus, we carry-out all the Cases b-d as in Case-1.
- **Case-3** If  $m = 2$ :  
We have only two points in the geodesic, thus, we perform Cases c-d as in Case-1.

We use the smoothing parameter  $s$  to offset the spline fit between no fitting error (when  $s = 0$ ) and the best smoothness (when  $s \rightarrow \infty$ ). The parameter  $s$  controls the sum of square errors between the training points and the fitted function. The best value for  $s$  ensuring the least error while having a sufficient smoothness is bounded by a function of the number of points in the geodesic as

$$m - \sqrt{m} \leq s \leq m + \sqrt{m}, \quad (10)$$

[29]. Since the number of points in geodesics vary, we are unable to input a onetime value as the smoothing parameter into the method that satisfies the inequality (10). In order to control this, here we introduce a new parameter called the smoothing multiplier  $\mu_s \geq 0$  such that  $s = \mu_s m$ . Now, given  $\mu_s$ , SGE uses different smoothing parameters for different smooth geodesics depending on  $m$ .

For each pair of point indices  $i, j$  in the dataset, we execute the aforesaid procedure and approximate the length of the smooth geodesic  $d_{i,j}$ . Then, we square the entries  $d_{i,j}$  and create the matrix  $\mathbf{D} = [d_{i,j}^2]_{n \times n}$ . We perform double

centering on  $\mathbf{D}$  using Eqn. (1) to obtain the doubly centered matrix  $\mathbf{S}$ . Then, we compute SVD as in Eqn. (4) followed by computing  $p$ -dimensional latent variables  $\hat{\mathbf{X}}$  according to Eqn. (3). A summary of the method SGE is presented in Algorithm 1.

## 4 PERFORMANCE ANALYSIS

In this section we demonstrate the effectiveness of our proposed NDR approach using three representative examples. As the first example, we use a synthetic dataset of a semi-sphere to analyze the performance of SGE with respect to neighborhood size, smoothness, sparsity, and noise. Then, we study the performance of SGE using two standard benchmark datasets: 1) face images [30]; and 2) images of handwritten digits (2's, 4's, 6's, and 8's) [31].

### 4.1 Embedding of a semi-sphere

We begin by embedding a synthetic dataset sampled from a semi-spherical manifold using SGE and Isomap to demonstrate the key concepts of our proposed SGE technique since, in this case, we can analytically compute the manifold distance on the semi-sphere and then compare with the embedding distances computed by SGE and Isomap. We sample 600 points from the manifold defined by

$$\begin{aligned} y_1 &= r \cos(\gamma_1) \cos(\gamma_2), \\ y_2 &= r \cos(\gamma_1) \sin(\gamma_2), \\ y_3 &= r \sin(\gamma_1), \end{aligned} \quad (11)$$

for  $\gamma_1 = \mathcal{U}[-\pi/2, \pi/2]$  and  $\gamma_2 = \mathcal{U}[0, \pi]$  where  $\mathcal{U}[a, b]$  denotes a uniform distribution between  $a$  and  $b$ . Here,  $r$  is the radius of the semi-sphere which is set to  $20 + \mathcal{N}[0, 3^2]$ , where  $\mathcal{N}[0, 3^2]$  is a random variable sampled from a Gaussian distribution with mean 0 and variance  $3^2$ . Here, we impose a high noise into the dataset as we are going to investigate the robustness of our method of embedding noisy datasets.

We set the spline threshold  $\nu$  and spline discretization  $h$  to be 10% and 100, respectively. Then, we run the SGE algorithm repeatedly over the spherical dataset with  $\delta = 2, 3, \dots, 8$ ;  $\mu_s = 0, 0.1, \dots, 1.0$  and obtain two-dimensional embeddings. Here, we have 77 different pairs of  $\delta$ 's and  $\mu_s$ 's, those then produce 77 two-dimensional embeddings. Now, we assess the performance of the methods in terms of distance preserving ability between the original data and the embedding. For each such embedding (77 in total), we compute distances between points in the embedding space using the Euclidean metric and denote the distance matrix by  $\mathbf{D}_S$ . Now, we run Isomap with the same sequence of  $\delta$ 's above and obtain its two-dimensional embeddings. The distance matrix for the embedding of Isomap is denoted by  $\mathbf{D}_I$ . Now, we compute true manifold distances between points of the dataset using cosine distances. If  $\alpha$  and  $\beta$  are two points on a semi-sphere with radius  $r$ , the manifold distance  $d$  is given by

$$d = r\gamma; \quad \gamma = \cos^{-1} \left( \frac{\alpha\beta}{|\alpha||\beta|} \right), \quad (12)$$

[32]. We compute all the pairwise distances using the above equation and form the distance matrix  $\mathbf{D}_M$  for the manifold.

**Algorithm 1** Smooth Geodesics Embedding (SGE).

*Inputs:* Data ( $\mathbf{Y}$ ), number of nearest neighbors ( $\delta$ ), smoothing multiplier ( $\mu_s$ ), spline threshold percentage ( $\nu$ ), number of discretizations ( $h$ ), and embedding dimension ( $p$ ).

*Outputs:* List of  $p$  largest singular values ( $\lambda_l; l = 1, \dots, p$ ) and  $p$ -dimensional embedding ( $\hat{\mathbf{X}}$ ).

- 1: For each point in  $\mathbf{Y}$ , choose  $\delta$  nearest points as neighbors [21].
- 2: Consider all the point in  $\mathbf{Y}$  as nodes and if any two nodes are chosen to be neighbors in 1, then join them by an edge having the length equal to the squared Euclidean distance between them. This step converts the dataset into a graph.
- 3: For each pair of nodes in the graph, find the points  $\mathcal{G} = \{\mathbf{y}_k | k = 1 \dots, m\}$  in the shortest path using Floyd's algorithm [23]. Here,  $m = |\mathcal{G}| \geq 2$ .
- 4: The points in  $\mathcal{G}$  are fitted with a smoothing spline and its length is computed:
  - Case-1 ( $m \geq 4$ ):
    - Case-a:
      - fit  $\mathcal{G}$  with a cubic smoothing spline using Eqn. (6) and Eqn. (7), then approximate the length  $d_{\hat{\mathcal{G}}}$  of that using Eqn. (8). Let, the length of the geodesic is  $d_G$  [Eqn. (9)]. If  $d_{\hat{\mathcal{G}}} < d_G(100 + \nu)/100$ , then accept  $d_{\hat{\mathcal{G}}}$  as the length of the smooth geodesic, otherwise proceed to Case-b.
    - Case-b:
      - fit  $\mathcal{G}$  with a quadratic smoothing spline using Eqn. (6) and Eqn. (7). Approximate the length  $d_{\hat{\mathcal{G}}}$  of that spline using Eqn. (8). If  $d_{\hat{\mathcal{G}}} < d_G(100 + \nu)/100$ , then accept  $d_{\hat{\mathcal{G}}}$  as the length of the smooth geodesic, otherwise proceed to Case-c.
    - Case-c:
      - fit  $\mathcal{G}$  with a linear smoothing spline using Eqn. (6) and Eqn. (7). Approximate the length  $d_{\hat{\mathcal{G}}}$  of that spline using Eqn. (8). If  $d_{\hat{\mathcal{G}}} < d_G(100 + \nu)/100$ , then accept  $d_{\hat{\mathcal{G}}}$  as the length of the smooth geodesic, otherwise proceed to Case-d.
    - Case-d:
      - Consider  $d_G$  as the approximated length of the smooth geodesic.
  - Case-2 ( $m = 3$ ): Perform Cases b-d similarly as in Case-1.
  - Case-3 ( $m = 2$ ): Perform Cases c-d similarly as in Case-1.
- 5: Fill the distance matrix  $\mathbf{D} = [d_{ij}^2]_{n \times n}$  where  $d_{ij}$  is the length of the smooth geodesic between nodes  $i$  and  $j$  computed in 3-4. Double center  $\mathbf{D}$  and convert it to a Gramian matrix  $\mathbf{S}$  using the Eqn. (1).
- 6: Perform the SVD on  $\mathbf{S}$  using Eqn. (4) and extract  $p$  largest singular values  $\lambda_l; l = 1, \dots, p$  along with the latent variable  $\hat{\mathbf{X}}$  as given by Eqn. (3).

The embedding error of SGE, denoted by  $\mathcal{E}_S$ , is computed as the Mean Absolute Deviation (MAD) between embedding and data [33]. Since the distance matrices are symmetric and have zeros on the diagonal, MAD can then be computed using

$$\mathcal{E}_S = \frac{2}{n(n-1)} \sum_{i=2}^n \sum_{j=i}^n |(D_R)_{ij} - (D_S)_{ij}|. \quad (13)$$

Similarly, for each pair of  $\delta$  and  $\mu_s$ , we also compute MAD between the embedding of Isomap and the original data that we denote by  $\mathcal{E}_I$ . Fig. 2 illustrates MADs for Isomap ( $\mathcal{E}_I$ ), SGE ( $\mathcal{E}_E$ ), and their differences ( $\mathcal{E}_I - \mathcal{E}_S$ ), versus  $\delta$  and  $\mu_s$ . Fig. 2(a) and 2(b) show that both methods display decreasing errors for increasing  $\delta$ 's (i.e., increasing neighbors), while SGE has decreasing error as  $\mu_s$  increases. Fig. 2(c) also indicates that SGE performs better than Isomap for larger smoothing multipliers for all  $\delta$ 's. Moreover, this plot shows SGE performs worst when  $\delta = 2$  and  $\mu_s = 0$ , and performs best when  $\delta = 2$  and  $\mu_s = 1$ .

Next, we analyze the influence of data sparsity of the manifold for embedding with SGE and compare that with Isomap. For that task, we produce a sequence of spherical datasets with an increasing number of points. We create the first dataset of 200 points using Eqn. (11) with  $r = 20 + \mathcal{N}[0, 2^2]$ , then add another 100 points, generated using the same equation, into the first dataset to produce

the second dataset. Similarly, we generate the last dataset of 1200 points. Then, we embed these datasets in two-dimensions using both Isomap with  $\delta = 3$  and SGE with  $\delta = 3$ ,  $\mu_s = 1$ , and  $\nu = 10\%$ . We compute the embedding errors  $\mathcal{E}_S$  and  $\mathcal{E}_I$  using MAD for each dataset as explained before. Since a significantly higher noise is used for the datasets, we run both methods over each dataset for 16 realizations to allow us to compute averages. Fig. 3(a) shows the mean of embedding errors of 16 realizations and error bars for the errors of Isomap and SGE embeddings. We observe that the error associated with SGE embedding is smaller than that of Isomap for all values of  $n$ .

Finally, we study the embedding error in terms of the size of the noise present in the data. For that task we formulate a latticed semi-sphere of 600 points using Eqn. (11) with equally appropriately discretized  $\gamma_1 \in [-\pi/2, \pi/2]$  and  $\gamma_2 \in [0, \pi]$ . Then, we impose increasing uniform noise levels into the parameter representing the radius as  $r = 20 + \eta \mathcal{U}[-1, 1]; \eta = 0, 0.3, 0.9, \dots, 3$  and produce 11 datasets. We embed each dataset 25 times (25 realizations) using Isomap with  $\delta = 3$  and SGE with  $\delta = 3$ ,  $\nu = 10\%$ , and  $\mu_s = 1$ . Fig. 3(b) presents embedding errors for both methods computed using Eqn. (13). We observe that, while  $\mathcal{E}_S$  slowly increases with increasing  $\eta$ ,  $\mathcal{E}_I$  increases more quickly with increasing  $\eta$ . Note that, the errorbars for  $\mathcal{E}_S$  are significantly smaller compared to that of  $\mathcal{E}_I$  at any given  $\eta$ .

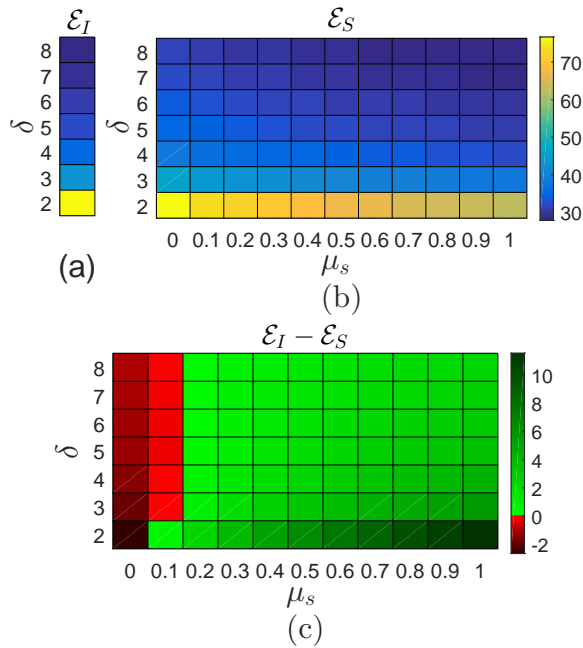


Fig. 2: Analyzing the performance of Isomap and SGE embeddings using Mean Absolute Deviation (MAD). Herein, we compute, (a) MAD between Isomap embedding and data, denoted by  $\mathcal{E}_I$ , for different neighborhood sizes ( $\delta$ 's), and (b) MAD between SGE embedding and data, denoted by  $\mathcal{E}_S$ , for different neighborhood sizes and smoothing multiplier ( $\mu_s$ 's). (c) The difference of errors between these two methods ( $\mathcal{E}_I - \mathcal{E}_S$ ) which is computed in the variable space  $\delta$  and  $\mu_s$ . The green cells denote that the performance of SGE is superior to that of Isomap.

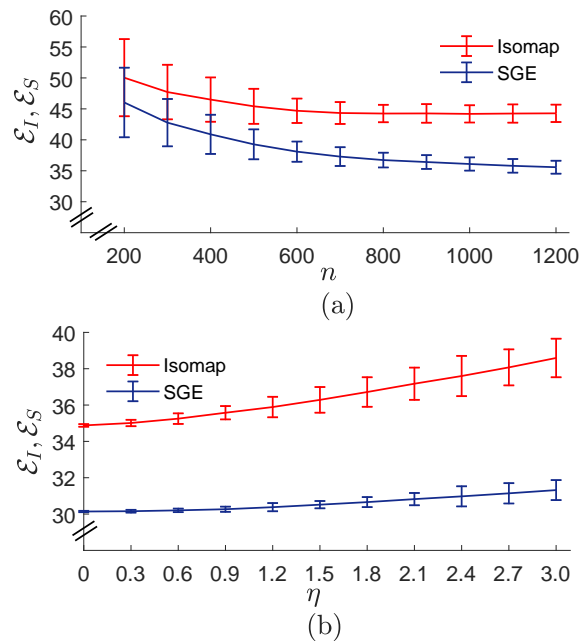


Fig. 3: Mean embedding error of Isomap, denoted by  $\mathcal{E}_I$ , (in red) and that of SGE, denoted by  $\mathcal{E}_S$ , (in blue) versus, (a) sparsity and (b) noise. Error bars represent standard deviations of errors computed over realizations. Note that, SGE has both lower average error and lower variance in the error across trials.

## 4.2 Embedding of face images

In this section, we validate the SGE method using a real-world dataset of face images available in [30]. This dataset consists 698 images of dimension  $64 \times 64$  each with a varying pose and direction of lighting, as shown by a sample of 16 snapshots in Fig. 4(a). We randomly choose 400 images as our baseline dataset and generate three other datasets of 400 images from the baseline dataset by imposing Gaussian noise with standard deviations ( $\sigma$ 's) 0.1, 0.2, and 0.3 [Fig. 4(b)]. We set  $\delta = 4$ ,  $\nu = 10\%$ ,  $h = 100$  in SGE and run this algorithm over each dataset (4 in total) 5 times for  $\mu_s = 0, 0.3, 0.6, 0.9, 1.2$ . Then, we embed these four datasets in two dimensions using Isomap with  $\delta = 4$ .

We use the ability to preserve distances between the original and the embedding data to analyze the performance of the method [34]. In particular, we view the distances in the original (noise free) imagery as the “true” distances and judge the algorithm’s ability to recover those distances after the imagery has been corrupted by noise. For both the data and the embedding, we first search  $\delta$  nearest neighbors for each point and then produce a weighted graph by treating points in the dataset as nodes and connecting each two neighbors by an edge having the length equal to their Euclidean distance. The weighted graph constructed through the nearest neighbor search is a simple graph<sup>2</sup> that does not contain self-loops or multiple edges. We compute the  $ij$ -th entry of the adjacency distance matrix  $A$  for the data as

$$A_{ij} = \begin{cases} d(i, j) & : \text{if } \exists \text{ an edge } ij \text{ in the graph} \\ & \text{of the original data,} \\ 0 & : \text{otherwise,} \end{cases} \quad (14)$$

and the  $ij$ -th entry of the adjacency distance matrix  $\tilde{A}$  for the embedding data as

$$\tilde{A}_{ij} = \begin{cases} d(i, j) & : \text{if } \exists \text{ an edge } ij \text{ in the graph} \\ & \text{of the embedding data,} \\ 0 & : \text{otherwise.} \end{cases} \quad (15)$$

Here,  $d(i, j)$  is the Euclidean distance between nodes  $i$  and  $j$ . In this paper, we impose Gaussian noise into real-world datasets such as face images and images of handwritten digits. Thus, we think of our original data as the uncorrupted data before we impose the noise.

For  $n$  points in the dataset, the error associated with the neighbors’ distance is computed as the normalized sum of pairwise absolute differences between entries of the adjacency distance matrices,

$$\text{error} = \frac{1}{n\delta} \sum_{i,j} |A_{ij} - \tilde{A}_{ij}|, \quad (16)$$

where  $\delta$  is the neighbor parameter [34].

Fig. 4(c) illustrates the embedding errors of Isomap, denoted by  $\mathcal{E}_I$ , and SGE, denoted by  $\mathcal{E}_S$ , for  $\sigma = 0, 0.1, 0.2, 0.3$  and  $\mu_s = 0, 0.3, 0.6, 0.9, 1.2$ . We observe that the error increases in both methods when the noise in the data increases. However, the error of embedding noisy data

2. A simple graph is an undirected graph that does not contain loops (edges connected at both ends to the same vertex) and multiple edges (more than one edge between any two different vertices) [35].

can be reduced significantly by choosing appropriate non-zero smoothing multipliers in SGE as shown here. Fig. 4(d) showing the difference of errors ( $\mathcal{E}_I - \mathcal{E}_S$ ) demonstrates that SGE performs better in terms of error than Isomap for all the noise levels with  $\mu_s \geq 0.3$ .

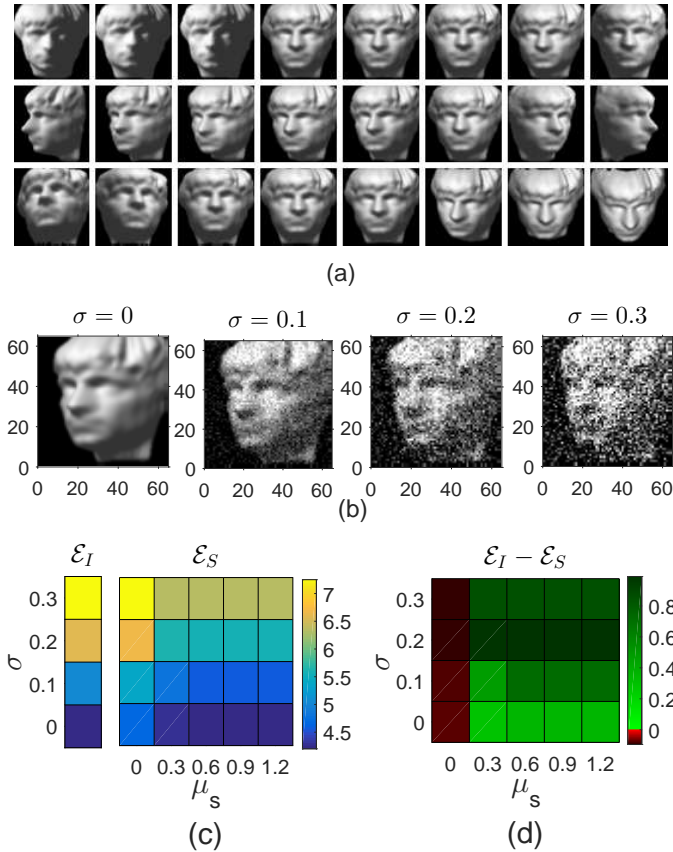


Fig. 4: Embedding of face images ( $64 \times 64$  dimensional), distorted with different noise levels, using Isomap and SGE with different smoothing levels. (a) A sample of 16 face images [30]; where the snapshots in the first, second, and third rows, represent left-right light change, left-right pose change, and up-down pose change, respectively. (b) Face images are distorted by imposing three levels of Gaussian noise  $\sigma = 0.1, 0.2,$  and  $0.3$ . The datasets (four in total) are embedded using Isomap and then using SGE with smoothing multipliers  $\mu_s = 0, 0.3, 0.6, 0.9, 1.2$ . Then, (c) the embedding errors of Isomap ( $\mathcal{E}_I$ ) and SGE ( $\mathcal{E}_S$ ), and (d) their error difference are computed. *The green cells denote that the performance of SGE is superior to that of Isomap.*

### 4.3 Embedding of handwritten digits

Next, we embed handwritten digits available from the Mixed National Institute of Standards and Technology (MNIST) database [31] using SGE and study the performance of the method on this dataset. This dataset contains 60,000  $28 \times 28$  dimensional images of handwritten digits from 0 to 9. We sample two arbitrary datasets for our study, each with 400 images, such that one dataset has only the digit 2 and the other dataset has the digits 2, 4, 6, and 8.

We run Isomap over the dataset having the digit 2 with  $\delta = 4$ . We run SGE two times: first with  $\delta = 4, \mu_s = 0, \nu = 10\%$ , and  $h = 100$ ; and second with  $\delta = 4, \mu_s = 0.6, \nu = 10\%$ , and  $h = 100$ . Thus, aforesaid procedure yields three two-dimensional embeddings. We formulate the adjacency distance matrices for the data and embedding using Eqns. (14) and (15), respectively, and compute the error of embedding using Eqn. (16). Then, we distort the dataset of 400 images with Gaussian noise having  $\sigma = 0.2$  and run Isomap with  $\delta = 4$ . We run the noisy dataset two times in SGE: first with parameters  $\delta = 4, \mu_s = 0, \nu = 10\%$ , and  $h = 100$ ; and second with  $\delta = 4, \mu_s = 0.6, \nu = 10\%$ , and  $h = 100$ . The embedding errors for Isomap, SGE with  $\mu_s = 0$ , and SGE with  $\mu_s = 0.6$ , are given in Table 1(a). We see in this table that, regardless of the noise present in the data, the error associated with SGE without smoothing is greater than that of Isomap, while that of SGE with smoothing is smaller than that of Isomap. Moreover, the error of embedding is increased when moving from the noisy dataset to the noise free dataset by .87 for Isomap, while that is only increased by .24 for SGE with  $\mu_s = 0.6$ . This is due to the fact that setting the smoothing parameter  $\mu$  to  $\mu_s = 0.6$  allows SGE to recover the manifold corrupted by noisy measurements.

Next, we embed a sample of 400 digits, consisting of 2's, 4's, 6's, and 8's, into two dimensions using Isomap and SGE. We run Isomap over this dataset with  $\delta = 4$ . Then, run SGE two times: first with  $\delta = 4, \nu = 10\%, \mu_s = 0,$  and  $h = 100$ ; and second with  $\delta = 4, \nu = 10\%, \mu_s = 0,$  and  $h = 100$ . Thereafter, we distort the dataset with a Gaussian noise having  $\sigma = 0.3$  and then run Isomap with  $\delta = 4$  followed by running SGE with the same two parameter sets that we used before. Then, we compute the Isomap and SGE errors associated with embedding of noise free and noisy datasets using Eqn. (16) that we present in Table 1(b). Similarly to the embedding of the digit 2, regardless of the error in the data, here we also note that the embedding error of SGE *with no smoothing* is greater than that of Isomap, while that of SGE *with smoothing* is smaller than that of Isomap. Moreover, moving from embedding of noise free data to embedding of noisy data, while the error associated with Isomap is increased by .88, that of SGE with  $\mu_s = 0.9$  is increased only by .21.

Finally, we compare the classification ability of both methods with the presence of high noise. In this dataset, clear clustering of similar digits allows for better classification accuracy. To demonstrate the desired clustering we present two dimensional Isomap and SGE embeddings of the noisy dataset ( $\sigma = 0.3$ ) of digits 2, 4, 6, and 8, that we present in Fig. 5. Therein, we observe that while Isomap is unable to achieve a clear clustering of digits, SGE with  $\mu_s = 0.9$  achieves qualitatively better clustering, even under the high noise present in the data.

## 5 CONCLUSION

Nonlinear dimensionality reduction methods can recover unfaithful embeddings due to presence of high noise in the data. In order to obtain a faithful embedding for noisy data, some smoothing procedure should be performed in the embedding. With this idea in mind, herein we introduced a

| (a)       | Noise          | Isomap | SGE         |               |
|-----------|----------------|--------|-------------|---------------|
|           |                |        | $\mu_s = 0$ | $\mu_s = 0.6$ |
| Digit "2" | $\sigma = 0$   | 7.02   | 7.13        | 5.86          |
|           | $\sigma = 0.2$ | 7.89   | 8.19        | 6.10          |

| (b)                              | Noise          | Isomap | SGE         |               |
|----------------------------------|----------------|--------|-------------|---------------|
|                                  |                |        | $\mu_s = 0$ | $\mu_s = 0.9$ |
| Digits "2", "4",<br>"6", and "8" | $\sigma = 0$   | 7.38   | 7.43        | 6.09          |
|                                  | $\sigma = 0.3$ | 8.20   | 8.36        | 6.30          |

TABLE 1: Errors of Isomap and SGE Embeddings of, (a) a sample of 400 handwritten 2's; and (b) a sample of 400 handwritten digits having number 2's, 4's, 6's, and 8's. The first row of (a) shows the error when the dataset of digit 2 is embedded using both Isomap, and SGE with two smoothing coefficients  $\mu_s = 0$  and  $\mu_s = 0.6$ . Then, the dataset is imposed with a Gaussian noise of  $\sigma = 0.2$  and embedded using both Isomap, and SGE with  $\mu_s = 0$  and  $\mu_s = 0.6$  that you see in the second row of (a). The first row of (b) represents the errors of Isomap embedding, and SGE embeddings with  $\mu_s = 0$  and  $\mu_s = 0.9$ , of the noise free version of the sample of digits having the numbers 2, 4, 6, and 8. The second row of (b) represents the errors of Isomap embedding, and SGE embeddings with  $\mu_s = 0$  and  $\mu_s = 0.9$ , of the noisy version of the dataset created by imposing a Gaussian noise with  $\sigma = 0.3$ .

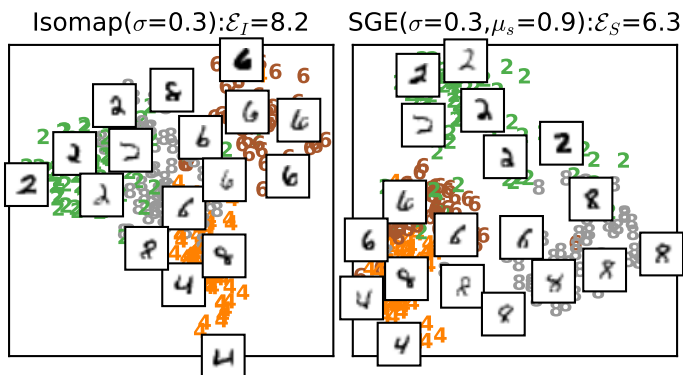


Fig. 5: Isomap and SGE Embeddings of handwritten numbers 2, 4, 6, and 8. Different digits are shown in different colors (2's in green, 4's in orange, 6's in brown, and 8's in gray) in the two-dimensional embedding space and the embedded snapshots illustrate the appearance of arbitrarily chosen handwritten digits. The left panel shows the Isomap embedding of the noisy dataset ( $\sigma = 0.3$ ) and the right panel shows the SGE embedding of the same dataset with  $\mu_s = 0.9$ . The embedding error of each case is indicated in the title of the corresponding panel. Note that, qualitatively speaking, the SGE embedding appears to have better clustering of similar digits than that of Isomap.

novel nonlinear dimensionality reduction framework using smooth geodesics that emphasizes the underlying smoothness of the manifold. Our method begins by first searching for nearest neighbors for each point using a  $\delta$ -nearest neighbor search [21]. Then, we create a weighted graph by representing all of the points as nodes and joining neighboring nodes with edges having their Euclidean distances as weights. For each pair of nodes in the graph, we create a geodesic [14], that is defined as the shortest path between the given nodes generated using Floyd's algorithm [36]. We fit each such geodesic with a smoothing spline (called a smooth geodesic) with smoothing multiplier ( $\mu_s$ ) and spline threshold ( $\nu$ ) [28], [29]. The length of these splines are treated as manifold distances between corresponding points. Finally, we use the classic MDS method to find the dimension of the distance matrix of smooth geodesics and perform the embedding.

In SGE, the order of the spline fit is set to either three, two, or one, depending on the spline threshold. Since a sufficient smoothness and a low fitting error can be obtained by cubic smoothing splines, we first rely on a spline fit of order three. However, we observed that the smoothing spline routing in [28] fits very long cubic splines for some specific smoothing multipliers. Thus, if the length of a cubic smoothing spline doesn't satisfy the threshold, we reduce the order of the spline to the next level.

We first demonstrated the effectiveness of our technique on a synthetic dataset representing a section of a semi-sphere. We observed that smoothing approach provides better performance than what is achieved by standard Isomap when embedding a noisy dataset. We also observed that the errors in both methods decrease as the neighborhood size increases [Fig. 2(a) and (b)]. However, when the neighborhood size is small, say  $\delta = 2$ , SGE has clear performance advantages over Isomap for noisy data when a sufficient smoothness is employed [Fig. 2(c)]. The spherical dataset also demonstrated that SGE is more robust to sparse sampling than Isomap [Fig. 3(a)]. Moreover, while increasing noise in the data always appears to reduce the performance of the embedding, irrespective to the method that is used, we see that Isomap is highly effected by increasing noise while SGE, with a judicious choice of smoothing parameter, is more robust [Fig. 3(b)].

We also studied two standard benchmark data sets, face images and handwritten digit images, and found that SGE provided similar superior performance on noisy versions of those data sets. In particular, for the digit classification task, we observed that SGE provides qualitatively superior clustering of similar digits in the presence of noise. As future work, we will quantify the classification performance of the low dimensional nonlinear embedding using a variety of standard supervised machine learning techniques.

The NDR method that we introduced here ensures better performance and preserves the topology of the manifold by emphasizing the smoothness of the manifold when embedding noisy data. This method is an extension of famous NDR method Isomap where we replaced the geodesics with smoothing splines. In the future, we plan to examine such techniques in more generality. For example, one can imagine generalizing Isomap to the case where geodesics are not a good approximation of long manifold distances. In such a



case, one can attempt to treat the long manifold distances as unknown, and employ matrix completion techniques on distance matrices where some entries are not observed.

## ACKNOWLEDGMENTS

The author's would like to thank Chen Zou for the support given in coding and also would like to thank the NSF XSEDE Jetstream [37], [38] under allocation TG-DMS160019 for support of this work.

## REFERENCES

- [1] R. Daley, *Atmospheric data analysis*. Cambridge university press, 1993, no. 2.
- [2] D. A. Jones, W. Wang, and R. Fawcett, "High-quality spatial climate data-sets for australia," *Australian Meteorological and Oceanographic Journal*, vol. 58, no. 4, p. 233, 2009.
- [3] B. S. Manjunath and W.-Y. Ma, "Texture features for browsing and retrieval of image data," *IEEE Transactions on pattern analysis and machine intelligence*, vol. 18, no. 8, pp. 837–842, 1996.
- [4] J. Zumberge, M. Heflin, D. Jefferson, M. Watkins, and F. H. Webb, "Precise point positioning for the efficient and robust analysis of gps data from large networks," *Journal of Geophysical Research: Solid Earth*, vol. 102, no. B3, pp. 5005–5017, 1997.
- [5] P. J. Carrington, J. Scott, and S. Wasserman, *Models and methods in social network analysis*. Cambridge university press, 2005, vol. 28.
- [6] R. Becker, R. Cáceres, K. Hanson, S. Isaacman, J. M. Loh, M. Martonosi, J. Rowland, S. Urbanek, A. Varshavsky, and C. Volinsky, "Human mobility characterization from cellular network data," *Communications of the ACM*, vol. 56, no. 1, pp. 74–82, 2013.
- [7] D. W. Huang, B. T. Sherman, and R. A. Lempicki, "Systematic and integrative analysis of large gene lists using david bioinformatics resources," *Nature protocols*, vol. 4, no. 1, pp. 44–57, 2009.
- [8] J. Schäfer and K. Strimmer, "An empirical bayes approach to inferring large-scale gene association networks," *Bioinformatics*, vol. 21, no. 6, pp. 754–764, 2005.
- [9] K. Gajamannage, S. Butail, M. Porfiri, and E. M. Bollt, "Identifying manifolds underlying group motion in vicsek agents," *The European Physical Journal Special Topics*, vol. 224, no. 17–18, pp. 3245–3256, 2015.
- [10] K. Gajamannage and E. M. Bollt, "Detecting phase transitions in collective behavior using manifold's curvature," *Mathematical Biosciences and Engineering*, vol. 14, no. 2, pp. 437–453, 2017.
- [11] L. Van Der Maaten, E. Postma, and J. Van den Herik, "Dimensionality reduction: a comparative," *J Mach Learn Res*, vol. 10, pp. 66–71, 2009.
- [12] I. Jolliffe, *Principal component analysis*. Wiley Online Library, 2002.
- [13] T. F. Cox and M. A. Cox, *Multidimensional scaling*. CRC press, 2000.
- [14] J. B. Tenenbaum, V. De Silva, and J. C. Langford, "A global geometric framework for nonlinear dimensionality reduction," *science*, vol. 290, no. 5500, pp. 2319–2323, 2000.
- [15] P. DeLellis, G. Polverino, G. Ustuner, N. Abaid, S. Macri, E. M. Bollt, and M. Porfiri, "Collective behaviour across animal species," *Scientific reports*, vol. 4, p. 3723, 2014.
- [16] M. H. Yang, "Face recognition using extended isomap," in *International Conference on Image Processing*, vol. 2. IEEE, 2002, pp. 117–120.
- [17] —, "Extended isomap for pattern classification," in *AAAI/IAAI*, 2002, pp. 224–229.
- [18] M. Balasubramanian and E. L. Schwartz, "The isomap algorithm and topological stability," *Science*, vol. 295, no. 5552, pp. 7–7, 2002.
- [19] J. A. Lee, A. Lendasse, M. Verleysen *et al.*, "Curvilinear distance analysis versus isomap," in *ESANN*, vol. 2, 2002, pp. 185–192.
- [20] H. Zha and Z. Zhang, "Isometric embedding and continuum isomap," in *ICML*, 2003, pp. 864–871.
- [21] J. H. Friedman, J. L. Bentley, and R. A. Finkel, "An algorithm for finding best matches in logarithmic expected time," *ACM Transactions on Mathematical Software (TOMS)*, vol. 3, no. 3, pp. 209–226, 1977.
- [22] P. K. Agarwal, J. Erickson *et al.*, "Geometric range searching and its relatives," *Contemporary Mathematics*, vol. 223, pp. 1–56, 1999.
- [23] R. W. Floyd, "Algorithm 97: shortest path," *Communications of the ACM*, vol. 5, no. 6, p. 345, 1962.
- [24] S. Xiang, F. Nie, C. Zhang, and C. Zhang, "Nonlinear dimensionality reduction with local spline embedding," *IEEE Transactions on Knowledge and Data Engineering*, vol. 21, no. 9, pp. 1285–1298, 2009.
- [25] K. Gajamannage, S. Butail, M. Porfiri, and E. M. Bollt, "Dimensionality reduction of collective motion by principal manifolds," *Physica D: Nonlinear Phenomena*, vol. 291, pp. 62–73, 2015.
- [26] J. A. Lee and M. Verleysen, *Nonlinear dimensionality reduction*. Springer Science & Business Media, 2007.
- [27] E. W. Dijkstra, "A note on two problems in connexion with graphs," *Numerische mathematik*, vol. 1, no. 1, pp. 269–271, 1959.
- [28] C. De Boor, "On calculating with b-splines," *Journal of Approximation theory*, vol. 6, no. 1, pp. 50–62, 1972.
- [29] C. H. Reinsch, "Smoothing by spline functions," *Numerische mathematik*, vol. 10, no. 3, pp. 177–183, 1967.
- [30] Deep learning. [Online]. Available: <http://deeplearning.net/datasets/>
- [31] Y. LeCun, C. Cortes, and C. J. Burges. The mnist database of handwritten digits. [Online]. Available: <http://yann.lecun.com/exdb/mnist/>
- [32] J. Stewart, *Essential calculus: Early transcendentals*. Cengage Learning, 2012.
- [33] J. D. Petrucci, B. Nandram, and M. Chen, *Applied statistics for engineers and scientists*. Prentice Hall New Jersey, 1999.
- [34] B. Shaw and T. Jebara, "Structure preserving embedding," in *Proceedings of the 26th Annual International Conference on Machine Learning*. ACM, 2009, pp. 937–944.
- [35] R. Balakrishnan and K. Ranganathan, *A textbook of graph theory*. Springer Science & Business Media, 2012.
- [36] T. H. Cormen, *Introduction to algorithms*. MIT press, 2009.
- [37] C. A. Stewart, T. M. Cockerill, I. Foster, D. Hancock, N. Merchant, E. Skidmore, D. Stanzione, J. Taylor, S. Tuecke, G. Turner *et al.*, "Jetstream: A self-provisioned, scalable science and engineering cloud environment," in *Proceedings of the 2015 XSEDE Conference: Scientific Advancements Enabled by Enhanced Cyberinfrastructure*. ACM, 2015, p. 29.
- [38] J. Towns, T. Cockerill, M. Dahan, I. Foster, K. Gaither, A. Grimshaw, V. Hazlewood, S. Lathrop, D. Lifka, G. D. Peterson *et al.*, "Xsede: accelerating scientific discovery," *Computing in Science & Engineering*, vol. 16, no. 5, pp. 62–74, 2014.



**Kelum Gajamannage** Dr. Kelum Gajamannage was awarded his BS (with honor) in Mathematics and MS in Applied Statistics from University of Peradeniya, Sri Lanka. He worked three years as a lecturer in the Department of Science and Technology at Uva Wellassa University, Sri Lanka. Dr. Gajamannage graduated with a PhD in Mathematics at Clarkson University, USA. He is currently a PostDoctoral Scholar in the department of Mathematical Sciences, Worcester Polytechnic Institute, USA.



**Randy Paffenroth** Dr. Paffenroth graduated from Boston University with degrees in both mathematics and computer science and he was awarded his Ph.D. in Applied Mathematics from the University of Maryland in June of 1999. After attaining his Ph.D., Dr. Paffenroth spent seven years as a Staff Scientist in Applied and Computational Mathematics at the California Institute of Technology. In 2006, he joined Numerica Corporation where he held the position of Computational Scientist and Program Director. Dr.

Paffenroth is currently an Associate Professor of Mathematical Sciences and Associate Professor of Computer Science at Worcester Polytechnic Institute where his focus is on the WPI Data Science Program. His current technical interests include machine learning, signal processing, large scale data analytics, compressed sensing, and the interaction between mathematics, computer science and software engineering, with a focus on applications in cyber-defense.



**Erik M. Bollt** Dr. Erik Bollt was awarded his Ph.D. in Mathematics from the University of Colorado in Boulder. Currently, he is a Full Professor at Clarkson University and endowed as the W. Jon Harrington Professor of Mathematics. Professor Bollt specializes in dynamical systems, chaos theory and turbulence, including as informed by data and signal processing, and remote sensing of the world's oceans, as well as inverse problems in data processing and information theoretic questions for information flow

and systems inference. Prof. Bollt has recently published a book on these topics as applied to systems such as the Gulf of Mexico oil spill, [Applied and Computational Measurable Dynamics, Book Publisher: Society for Industrial and Applied Mathematics, (2013)].